

## ABS: AN ANALYTICAL METHOD OF BLIND SEPARATION OF CMB FROM FOREGROUNDS

PENGJIE ZHANG<sup>1,2,3,4</sup>, JUN ZHANG<sup>1,4</sup>, LE ZHANG<sup>1,4</sup>

<sup>1</sup>DEPARTMENT OF ASTRONOMY, SCHOOL OF PHYSICS AND ASTRONOMY, SHANGHAI JIAO TONG UNIVERSITY, 955 JIANCHUAN ROAD, SHANGHAI, 200240

<sup>2</sup>IFSA COLLABORATIVE INNOVATION CENTER, SHANGHAI JIAO TONG UNIVERSITY, SHANGHAI 200240, CHINA

<sup>3</sup>TSUNG-DAO LEE INSTITUTE, SHANGHAI 200240, CHINA

<sup>4</sup>SHANGHAI KEY LABORATORY FOR PARTICLE PHYSICS AND COSMOLOGY

*Draft version December 12, 2017*

### ABSTRACT

Extracting CMB B-mode polarization from complicated foregrounds is a challenging task in searching for inflationary gravitational waves. We propose the ABS method as a blind and analytical solution to this problem. It applies to the measured cross bandpower between different frequency bands and obtains the CMB B-mode bandpower analytically. It does not rely on assumptions of foregrounds and does not require multiple parameter fitting. Testing against a variety of foregrounds, survey frequency configurations and instrument noise, we verify its applicability and numerical stability. The ABS method also applies to CMB temperature, E-mode polarization, the thermal Sunyaev Zel'dovich effect, spectral distortion, and even significantly different problems such as cosmic magnification.

*Keywords:* Cosmology: inflation:cosmic microwave background

### 1. INTRODUCTION

Searching for inflationary gravitational waves (Starobinskiĭ 1979) through the induced CMB B-mode polarization (Seljak & Zaldarriaga 1997; Seljak 1997; Kamionkowski et al. 1997) is a major endeavour of cosmology (e.g. BICEP: BICEP2 Collaboration et al. (2014); Grayson et al. (2016); BICEP2/Keck and Planck Collaborations et al. (2015); ACTpol: Thornton et al. (2016); SPTpol: Keisler et al. (2015); POLARBEAR: Inoue et al. (2016); PIPER: Gandilo et al. (2016); CORE: Delabrouille et al. (2017); EPIC: Bock et al. (2008); LiteBIRD: Matsumura et al. (2014); PIXIE: Kogut et al. (2011); PRISM: André et al. (2014); AliCPT: Li et al. (2017)). It will open a window into the very beginning of our universe.

A major challenge of CMB B-mode detection is to accurately remove polarized galactic foregrounds (Planck Collaboration et al. 2015b,a,c). At CMB frequency of  $\sim 100$  GHz, a major foreground is the galactic thermal dust, which likely dominates over CMB B-mode at  $\nu \gtrsim 100$  GHz, even for the cleanest sky areas (BICEP2/Keck and Planck Collaborations et al. 2015). Synchrotron emission may be another major foreground, especially at lower frequency. Other polarized foregrounds such as spinning dust (Planck Collaboration et al. 2011, 2015b) and magnetic dust (Draine & Hensley 2012; Planck Collaboration et al. 2015d) may also be non-negligible.

Usually CMB experiments rely on multi-frequency information to remove foregrounds (e.g. Planck Collaboration et al. (2015b,a,c); Kogut et al. (2011); André et al. (2014)). This kind of approaches faces various uncertainties. First, the exact frequency dependences of foregrounds and the exact number of

independent foreground components are unknown. For example, recently Planck found that dust foregrounds at 217 and 353 GHz bands are decorrelated at a few percent level, meaning the existence of multiple dust components. This may lead to a significant bias in  $r$  (tensor-to-scalar ratio) (Remazeilles et al. 2016; Planck Collaboration et al. 2016a; Poh & Dodelson 2016). To avoid such potential bias, alternative methods have been constructed (e.g. Tegmark et al. (2003); Delabrouille et al. (2003); Cardoso et al. (2008)) and applied (e.g. Planck Collaboration et al. (2015a)). For example, SMICA (Delabrouille et al. 2003; Cardoso et al. 2008) simultaneously fits many unknown parameters of CMB and foregrounds against the power spectrum measurements of all frequency bands and multipole bins. It has been successfully applied to the Planck data (e.g. Planck Collaboration et al. (2015a)). Nevertheless, it is computationally challenging due to the large number of fitting parameters. When applied to data analysis such as Planck, various assumptions such as the scale dependence of foreground spectra are often made (e.g. Planck Collaboration et al. (2015a)).

Here we report the **ABS** method, which stands for the **A**nalytical method of **B**lind **S**eparation of CMB from foregrounds. It can be treated as post-processing on the matrix of cross bandpower between frequency bands, which are heavily compressed products of the original (noisy) maps. It works on any single multipole bin. Due to the fact that CMB B-mode has a known (black-body) frequency dependence, a set of specific linear algebra operations on this measured matrix automatically returns the bandpower  $\mathcal{D}_B(\ell)$ , the most important B-mode statistics. The measurement procedure is completely fixed by the measured matrix and survey specifications, with no assumptions on foregrounds. Since it does not rely on fitting procedures, it is numerically stable and fast.

This paper is organized as follows. In §2 we describe the ABS method. In §3 we generate simulated data with

various foreground components, CMB B-mode, survey frequency configurations and instrumental noise. In §4 we test the ABS method against these simulated data. In §5 we derive the necessary and sufficient survey conditions for unbiased CMB measurement. We discuss and conclude in §6. The appendix contains proof of a few key results.

## 2. THE ABS METHOD

The ABS method is motivated by the analytical solution of  $\mathcal{D}_B$  derived under the ideal case of no instrument noise (§2.1). It is then extended to the case with instrument noise (§2.2).

### 2.1. The analytical solution for the case of no instrument noise

Our method works on  $\mathcal{D}_{ij}(\ell)$ , the  $N_f \times N_f$  matrix of cross bandpower between the  $i$ -th and  $j$ -th frequency band. Here  $\ell$  denotes the multipole bin.  $i, j = 1, 2 \dots N_f$  and  $N_f$  is the total number of frequency bands. In thermodynamic units,

$$\mathcal{D}_{ij}(\ell) = f_i^B f_j^B \mathcal{D}_B(\ell) + \mathcal{D}_{ij}^{\text{fore}}(\ell). \quad (1)$$

Since we use the thermodynamic units,  $f^B = 1$ .  $\mathcal{D}_{ij}^{\text{fore}}$  is the cross bandpower matrix of foreground. It has order  $N_f$ , but its rank  $M$  depends on the number of independent foreground components. Our task is to solve Eq. 1 for  $\mathcal{D}_B(\ell)$ , without assumptions of  $\mathcal{D}_{ij}^{\text{fore}}$ . This may appear as a mission impossible. However, due to the fact that CMB has a blackbody spectrum, and the fact that there may be limited foreground components in frequency space, Eq. 1 may be indeed solvable. We are able to prove the following two key results.

- **The solution to  $\mathcal{D}_B$  is unique, as long as  $M < N_f$ .** The proof is given in the appendix.
- **The analytical solution exists, given by**

$$\mathcal{D}_B = \left( \sum_{\mu=1}^{M+1} G_\mu^2 \lambda_\mu^{-1} \right)^{-1}. \quad (2)$$

Here the  $\mu$ -th eigenmode has eigenvector  $\mathbf{E}^{(\mu)}$  and eigenvalue  $\lambda_\mu$ . We adopt the normalization  $\mathbf{E}^{(\mu)} \cdot \mathbf{E}^{(\mu)} = 1$ .  $G_\mu \equiv \mathbf{f}^B \cdot \mathbf{E}^{(\mu)}$ . We rank the eigenmodes with decreasing order in  $\lambda_\mu$ . Since  $\mathcal{D}_{ij}$  is positive definite,  $\lambda_\mu > 0$ . The derivation of Eq. 2 is given in the appendix.

Eq. 2 is not straightforward to understand. However, for the limiting case of  $M \leq 2$ , one can solve for all eigenmodes analytically and verify Eq. 2 by brute-force. This equation also confirms our intuition that foreground components orthogonal to the CMB signal in the frequency space should not interfere CMB reconstruction.

Eq. 2 is not the only analytical expression for  $\mathcal{D}_B$ . A set of expression is as follows,

$$\mathcal{D}_B = \left( \sum_{\mu=1}^{M+1} G_\mu^2 \lambda_\mu^{-1} \right)^{-1}_{\mathcal{D}_{ij} + \mathcal{S} f_i^B f_j^B} - \mathcal{S}. \quad (3)$$

The shift parameter  $\mathcal{S}$  is a free parameter. It shifts the input value of CMB signal from  $\mathcal{D}_B$  to  $\mathcal{D}_B + \mathcal{S}$ .  $G_\mu$  and  $\lambda_\mu$

are defined with respect to the new matrix  $\mathcal{D}_{ij} + \mathcal{S} f_i^B f_j^B$ . Eq. 2 is a special case of Eq. 3 with  $\mathcal{S} = 0$ . If there are no instrument noises nor numerical errors, Eq. 2 & 3 are equivalent. However, in reality Eq. 3 with positive  $\mathcal{S}$  is more stable, more accurate and therefore more useful for the B-mode determination.

### 2.2. Extension to the case with instrument noise

The ensemble average of the instrument noise on the diagonal elements can be subtracted. What remain in the matrix are random noises  $\delta \mathcal{D}_{ij}^{\text{inst}}$ ,

$$\mathcal{D}_{ij}^{\text{obs}} \equiv \mathcal{D}_{ij} + \delta \mathcal{D}_{ij}^{\text{inst}}. \quad (4)$$

The residual noise has zero mean ( $\langle \delta \mathcal{D}_{ij}^{\text{inst}} \rangle = 0$ ). Different noise matrix elements are uncorrelated. The associated dispersion in each noise matrix element is  $\langle (\delta \mathcal{D}_{ij}^{\text{inst}})^2 \rangle = \sigma_{\mathcal{D},i}^{\text{inst}} \sigma_{\mathcal{D},j}^{\text{inst}} (1 + \delta_{ij})/2$ . Eq. 2 & 3 can still be implemented in the data analysis, with some modifications to account for instrument noise.

**Step 1.** First we need to deal with the varying  $\sigma_{\mathcal{D},i}^{\text{inst}}$  across frequency bands.<sup>1</sup> In this case, we should not treat each  $\mathcal{D}_{ij}^{\text{obs}}$  with equal weight. Instead, we should weigh  $\mathcal{D}_{ij}^{\text{obs}}$  by  $\sqrt{\sigma_{\mathcal{D},i}^{\text{inst}} \sigma_{\mathcal{D},j}^{\text{inst}}}$ ,

$$\mathcal{D}_{ij}^{\text{obs}} \rightarrow \tilde{\mathcal{D}}_{ij}^{\text{obs}} \equiv \frac{\mathcal{D}_{ij}^{\text{obs}}}{\sqrt{\sigma_{\mathcal{D},i}^{\text{inst}} \sigma_{\mathcal{D},j}^{\text{inst}}}}. \quad (5)$$

The ABS method applies to  $\tilde{\mathcal{D}}_{ij}^{\text{obs}}$ , with the following operations,

$$f_i^B \rightarrow \tilde{f}_i^B \equiv \frac{f_i^B}{\sqrt{\sigma_{\mathcal{D},i}^{\text{inst}}}},$$

$$G_\mu \rightarrow \tilde{G}_\mu \equiv \tilde{\mathbf{f}}^B \cdot \tilde{\mathbf{E}}^\mu, \quad \lambda_\mu \rightarrow \tilde{\lambda}_\mu. \quad (6)$$

Here  $\tilde{\mathbf{E}}^\mu$  is the  $\mu$ -th eigenvector of  $\tilde{\mathcal{D}}_{ij}^{\text{obs}}$  and  $\tilde{\lambda}_\mu$  is the eigenvalue. By such normalization, the noise matrix in  $\tilde{\mathcal{D}}_{ij}^{\text{obs}}$  has dispersion of 1 in the diagonal elements and  $1/\sqrt{2}$  in the off-diagonal elements.

**Step 2.** We also need to deal with unphysical eigenmodes induced by instrument noise. With the presence of instrument noise, the rank of  $\tilde{\mathcal{D}}_{ij}^{\text{obs}}$  will be  $N_f$ . The eigenmodes of instrument noises have typical amplitude  $\sim 1$  and their distribution is symmetric. Therefore we must exclude eigenmodes with negative eigenvalues. We should also exclude eigenmodes with small eigenvalues. We choose the threshold  $\lambda_{\text{cut}} \sim 1$ . We compute all  $N_f$  eigenmodes of  $\tilde{\mathcal{D}}_{ij}^{\text{obs}}$ , and then measure  $\mathcal{D}_B$  from Eq. 3, but only using eigenmodes with  $\tilde{\lambda}_\mu > \lambda_{\text{cut}}$ . Namely, the estimator of  $\mathcal{D}_B$  with the presence of instrument noise is

$$\hat{\mathcal{D}}_B = \left( \sum_{\tilde{\lambda}_\mu \geq \lambda_{\text{cut}}} \tilde{G}_\mu^2 \tilde{\lambda}_\mu^{-1} \right)^{-1}_{\tilde{\mathcal{D}}_{ij}^{\text{obs}} + \mathcal{S} \times \tilde{f}_i^B \tilde{f}_j^B} - \mathcal{S}. \quad (7)$$

<sup>1</sup> Real surveys have other complexities. The appendix §B will show that the ABS method is still applicable with the presence of masks and frequency dependent beams.

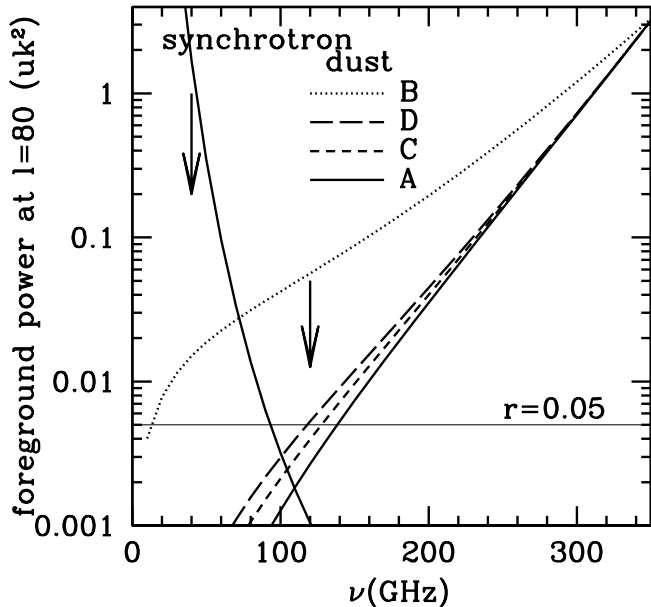


**Figure 1.** The foreground models for simulated observations to test the ABS method. The 4 models share identical synchrotron foreground, but different dust model parameters. Case C and D differ from case A and B by significant decorrelation between dust foregrounds at different frequencies. Case B and D have exaggerated dust contamination and are served to test the generality of our method.

**Step 3.** In this step we carry out a convergence test/self-calibration procedure to determine a suitable choice of  $\mathcal{S}$  and then use it to obtain  $\mathcal{D}_B$ .  $\mathcal{S}$  changes the distribution of physical eigenmodes. Larger positive  $\mathcal{S}$  makes the matrix operations more stable and the impact of instrument noise weaker. By increasing  $\mathcal{S}$  and finding the converged value of  $\hat{\mathcal{D}}_B$ , we obtain a more reliable measure of  $\mathcal{D}_B$ . We emphasize two points. First, both  $\mathcal{S}$  and  $\mathcal{D}_B$  are self-determined from the data and no extra uncertainties are introduced in this step. Second, this step is also necessary to pass the null test detailed later.

### 3. SIMULATED OBSERVATIONS FOR TESTS

Next we test the ABS method on simulated  $\mathcal{D}_{ij}^{\text{obs}}$  with a variety of foregrounds, instrument noise and survey frequency configurations.

#### 3.1. Foreground specifications

For foregrounds, we specify

$$\mathcal{D}_{ij}^{\text{fore}} = \sum_{\alpha=1}^M f_i^{(\alpha)} f_j^{(\alpha)} \mathcal{D}_\alpha. \quad (8)$$

$f_i^{(\alpha)} \equiv f^{(\alpha)}(\nu_i)$  is the frequency dependence of the  $\alpha$ -th foreground component and  $\mathcal{D}_\alpha$  is the bandpower amplitude. Throughout the paper, we include two polarized foregrounds (galactic dust and galactic synchrotron). When we consider decorrelation between galactic dust at different frequency, we need at least two  $f^\alpha(\nu)$  to describe dust alone. Therefore  $M = 2$  if no decorrelation and  $M \geq 3$  when decorrelation exists.

**Table 1**

We test our ABS method against various CMB frequency configurations and instrumental noise.  $\sigma_{\mathcal{D}}^{\text{inst}}$  is the r.m.s. error in the bandpower measurement caused by instrumental noise.

Labels	frequency/GHz	$\sigma_{\mathcal{D}}^{\text{inst}}/\mu\text{K}^2$
<b>F0</b>	30, 70, 100, 150, 217 & 353	(10 <sup>-5</sup> , 10 <sup>-2</sup> )
<b>F1</b>	95, 150, 220 & 270	
<b>F2</b>	35, 95, 150, 220 & 270	
<b>F3</b>	35, 95, 150, 220, 270 & 353	
<b>F4</b>	30, 36, 43, 51, 62, 75, 90, 105, 135 160, 185, 200, 220, 265, 300 & 320	

We consider four foreground models (case A, B, C, D, Fig. 1). They all share the same synchrotron foreground, but different dust foregrounds. For synchrotron,

$$f^{\text{syn}}(\nu) \propto \nu^{-\beta_{\text{syn}}/2} \frac{(e^x - 1)^2}{e^x x^4}, \quad \mathcal{D}_{\text{syn}} \propto \ell^{-0.6}. \quad (9)$$

Here  $\beta_{\text{syn}} = 3.3$  is the frequency index and  $x \equiv h\nu/(k_B T_{\text{CMB}})$ . The bandpower is normalized as  $3 \times 10^{-4} \mu\text{K}^2$ , at  $\nu = 150$  GHz and  $\ell = 80$ . This is the observationally allowed upper limit in the BICEP2 sky (BICEP2/Keck and Planck Collaborations et al. 2015).

For the galactic dust foreground, we adopt (Planck Collaboration et al. 2016b)

$$f^{\text{dust}}(\nu) \propto \frac{x^{\beta_d} (e^x - 1)^2}{x e^x (e^{x T_{\text{CMB}}/T_d} - 1)}, \quad \mathcal{D}_{\text{dust}} \propto \ell^{-0.42}. \quad (10)$$

To account for the recently detected decorrelation between different Planck frequency bands (Planck Collaboration et al. 2016a), we adopt a simple model of spatially stochastic variation in the dust index  $\beta_d$  (Planck Collaboration et al. 2016a). It induces a new component in  $\mathcal{D}_{ij}(\ell)$ ,

$$f^{\text{S}}(\nu) = f^{\text{dust}}(\nu) \times \ln(\nu/\nu_0), \quad \mathcal{D}_{\text{S}} = \mathcal{D}_{\text{dust}} A_{\text{S}}. \quad (11)$$

Here we adopt  $\nu_0 = 353$  GHz.  $A_{\text{S}} \propto \langle \delta\beta_d^2 \rangle$  is a free parameter to control the level of decorrelation. When this stochastic component is subdominant, the cross correlation coefficient between dust in  $i$ -th and  $j$ -th bands is  $\mathcal{R}_{\nu_i, \nu_j}^{\text{BB}} \simeq 1 - \frac{1}{2} A_{\text{S}} (\ln(\nu_i/\nu_j))^2$ . The overall bandpower is normalized as  $3.5 \mu\text{K}^2$  at  $\ell = 80$  and 353 GHz (BICEP2/Keck and Planck Collaborations et al. 2015).

We adopt 4 cases of dust parameters,  $(\beta_d, T_d, A_{\text{S}}) = (1.59, 19.6, 0.0)$ ,  $(0.5, 10, 0.0)$ ,  $(1.59, 19.6, 0.42)$ ,  $(1.59, 19.6, 0.84)$ . Case A is the best fit of Planck (Planck Collaboration et al. 2016b). Case B has a factor of 10 more dust contamination at 100-150 GHz than case A, and also a much flatter spectrum. Case C has dust decorrelation between frequency bands, reproducing the Planck finding of  $\mathcal{R}_{353, 217}^{\text{BB}} = 0.95$  (Planck Collaboration et al. 2016a). Case D has unrealistically large decorrelation (e.g.  $\mathcal{R}_{353, 150}^{\text{BB}} = 0.7$ ).

#### 3.2. Frequency configurations

Frequency configuration is crucial for foreground removal. We consider five configurations (**F0-F4**), shown in Table 1.

- **F0** is the fiducial one, with 6 bands centered at 30, 70, 100, 150, 217 & 353 GHz. This configuration is

similar to Planck. It has a wide frequency coverage, good for both synchrotron and dust foreground removal.

- **F1** has 4 bands at 95, 150, 220 & 270 GHz (Keck array-like, Grayson et al. (2016)). A major difference of **F1** to **F0** is the lack of low frequency bands and hence limited capability of synchrotron foreground identification and removal.
- **F2** adds a 35 GHz bands to **F1** (BICEP array-like, Grayson et al. (2016)). This is to test the gain adding a low frequency band.
- **F3** further adds a 353 GHz band to **F2**. This turns out to be important for dust foreground removal when decorrelation in dust foreground exists.
- **F4** has 16 bands between 30 GHz and 320 GHz. This is basically the frequency configuration of PRISM (André et al. 2014), expect that PRISM also has higher frequency bands. Other proposed space missions such as CORE, PIXIE and LiteBIRD have similar configurations.

### 3.3. B-mode signal and physical eigenmodes

For the CMB signal, we focus on  $\ell = 80$  around the recombination bump. The fiducial  $\mathcal{D}_B = 5 \times 10^{-3} \mu\text{K}^2$ , corresponding to the sum of  $r = 0.05$  and the lensing B-mode. We also consider  $\mathcal{D}_B = 2 \times 10^{-3} \mu\text{K}^2$  in which the lensing B-mode dominates. We further test around  $\ell = 5$  of the reionization bump, with the choices of  $\mathcal{D}_B = 1, 2 \times 10^{-3} \mu\text{K}^2$ .

The eigenmodes of  $\mathcal{D}_{ij}$  depend on foregrounds, CMB signal and observational frequency configuration. Two useful relations to understand these eigenmodes are

$$\begin{aligned} \sum_{\alpha=1}^{M+1} \lambda_{\alpha} &= \text{Tr} \mathcal{D}_{ij} = \sum_{i=1}^{N_f} \mathcal{D}_{ii}, \\ \sum_{\alpha=1}^{M+1} \lambda_{\alpha}^2 &= \sum_{ij} \mathcal{D}_{ij}^2. \end{aligned} \quad (12)$$

Fig. 2 shows the eigenmodes for foreground model C,  $\mathcal{D}_B = 5 \times 10^{-3} \mu\text{K}^2$ , and frequency configuration **F0**. It has 4 eigenmodes. The first two are essentially synchrotron and dust foreground, respectively. These can be seen from their frequency dependences (the shapes of eigenvectors). Furthermore,  $\lambda_1 \simeq \sum_i \mathcal{D}_{ii}^{\text{syn}} \sim \mathcal{D}_{11}^{\text{syn}}$ ,  $\lambda_2 \simeq \sum_i \mathcal{D}_{ii}^{\text{dust}} \sim \mathcal{D}_{66}^{\text{dust}}$ . The third one is dominated by CMB,  $\lambda_3 \simeq 5\mathcal{D}_B$ . It is close to  $N_f \mathcal{D}_B = 6\mathcal{D}_B$ , the limit of pure CMB B-mode. For the same reason, it contains non-negligible contamination from foregrounds. The fourth eigenmode is a mixture of CMB and foregrounds, with a frequency dependence resembling none of CMB and foregrounds. This eigenmode is also important for CMB measurement, as will be shown later.

### 3.4. Instrument noise specifications

To generate simulated  $\mathcal{D}_{ij}^{\text{obs}}$ , we approximate  $\delta \mathcal{D}_{ij}^{\text{inst}}$  as Gaussian random fields with dispersion  $\sigma_{\mathcal{D},ij}^{\text{inst}}$ . For brevity, we assume  $\sigma_{\mathcal{D},11}^{\text{inst}} = \sigma_{\mathcal{D},22}^{\text{inst}} = \dots = \sigma_{\mathcal{D}}^{\text{inst}}$  ( $i = 1, \dots, N_f$ ). Therefore  $\mathcal{D}_{ij}^{\text{obs}}$  and  $\tilde{\mathcal{D}}_{ij}^{\text{obs}}$  only differ by a

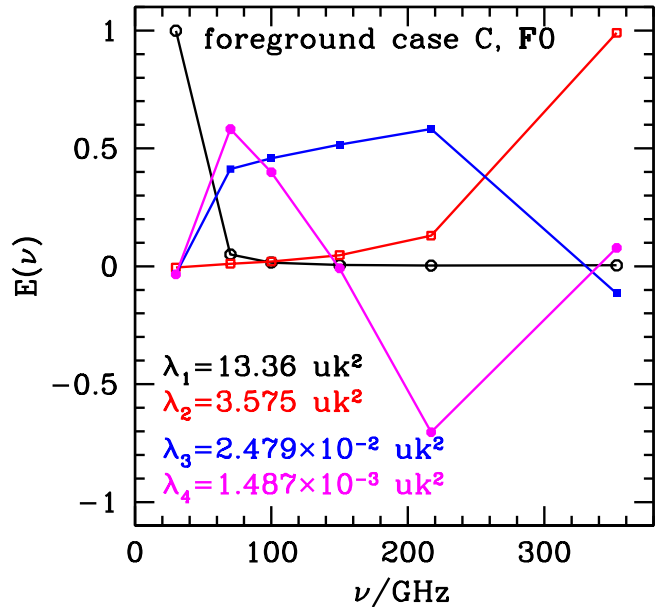


**Figure 2.** The eigenvectors and eigenvalues for foreground case C and frequency configuration **F0**, with  $\mathcal{D}_B = 5 \times 10^{-3} \mu\text{K}^2$  and centered at  $\ell = 80$ . Due to significant decorrelation of thermal dust foreground, case C has 4 eigenmodes. (1) The first eigenmode (open circle) is dominated by synchrotron foreground, with eigenvalue  $\lambda_1$  essentially its band power at 30 GHz. Since the synchrotron model is actually the observational upper limit, this eigenmode may be less significant in reality. (2) The second eigenmode (open square) is dominated by dust emission, with  $\lambda_2$  essentially the dust emission band power at 353 GHz. (3) The third eigenmode (filled square) is dominated by CMB B-mode. (4) The fourth eigenmode (filled circle) is a mixture of all foreground and CMB components. Although it is subdominant, it is important for unbiased CMB measurement.

uniform normalization. This allows us to work directly on  $\mathcal{D}_{ij}^{\text{obs}}$ , whose physical meaning is clearer than  $\tilde{\mathcal{D}}_{ij}^{\text{obs}}$ . Notice that the off-diagonal elements have smaller dispersion ( $\sigma_{\mathcal{D}}^{\text{inst}}/\sqrt{2}$ ).

Reducing instrument noise is a key task in CMB polarization experiments. BICEP2/Keck has reached  $\sigma_{\mathcal{D}}^{\text{inst}} \sim 10^{-3} \mu\text{K}^2$  (BICEP2/Keck and Planck Collaborations et al. 2015). Future experiments can go well below  $10^{-4} \mu\text{K}^2$ . For example, planned ground CMB-S4 projects (Abazajian et al. 2016) will have two orders of magnitude more detectors than BICEP2 ( $\sim 5 \times 10^5$ ) and therefore a factor of 10 reduction in instrument noise. PRISM (André et al. 2014) has typical noise  $\sim 70 \mu\text{K}/\text{detector}/\text{arcmin}^2$ ,  $\sim 200$  detectors per band,  $\sigma_{\mathcal{D}}^{\text{inst}} \simeq 3.7 \times 10^{-5} \mu\text{K}^2 (\ell/\Delta\ell)^{1/2} (0.5/f_{\text{sky}})^{1/2} (\ell/80)$ . Here  $\Delta\ell$  is the width of multipole bin and  $f_{\text{sky}}$  is the fractional sky coverage. Other experiments such as CORE (Delabrouille et al. 2017), EPIC and LiteBIRD have similar sensitivity. We consider a wide range of  $\sigma_{\mathcal{D}}^{\text{inst}} \in (10^{-5}, 10^{-2}) \mu\text{K}^2$  to include all these possibilities.

## 4. TESTING THE ABS METHOD

Fig. 3 shows the test result for the **F0** frequency configuration at  $\ell \sim 80$ . Throughout the paper, we fix the cut  $\lambda_{\text{cut}} = 1/2$ . Whether this choice of  $\lambda_{\text{cut}}$  is optimal and whether further improvement can be achieved are open

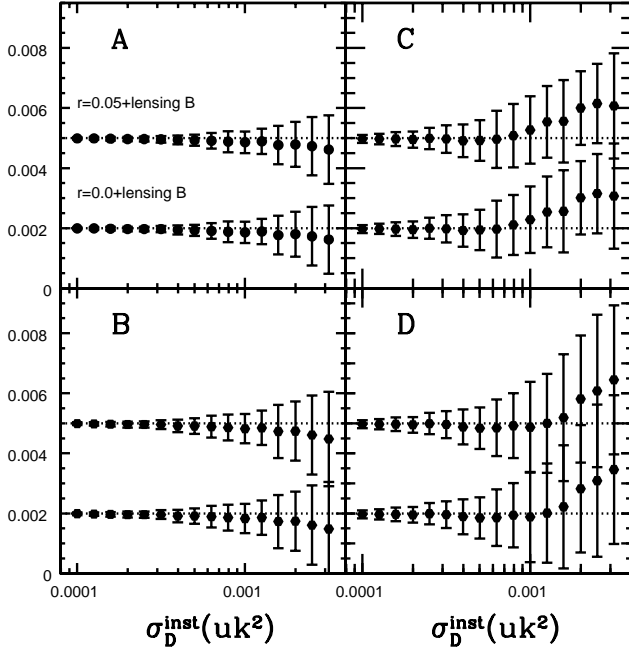


**Figure 3.** Tests for the F0 survey configuration and 4 cases of foregrounds. The  $y$ -axis is the bandpower in unit of  $\mu\text{K}^2$ . Dot lines are the input B-mode. Points are the ABS output, as a function of bandpower measurement error  $\sigma_{\mathcal{D}}^{\text{inst}}$ . The error bars are estimated using 200 realizations of instrument noise. The input  $\mathcal{D}_{\text{B}}$  is recovered unbiasedly. We emphasize that the adopted foreground cases are to generate simulated observational data. Our ABS method assumes nothing about these foregrounds.

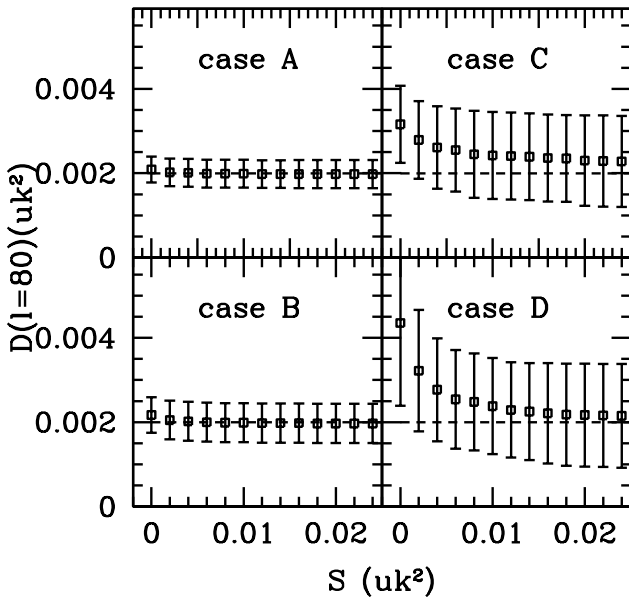


**Figure 4.** The convergence test and self-calibration process. We test the output  $\mathcal{D}_{\text{B}}$  as the function of  $\mathcal{S}$ , for  $\mathcal{D}_{\text{B}} = 2 \times 10^{-3} \mu\text{K}^2$  and  $\sigma_{\mathcal{D}}^{\text{inst}} = 10^{-3} \mu\text{K}^2$ . By choosing sufficiently large  $\mathcal{S}$ , systematic error in the reconstruction can indeed be alleviated.

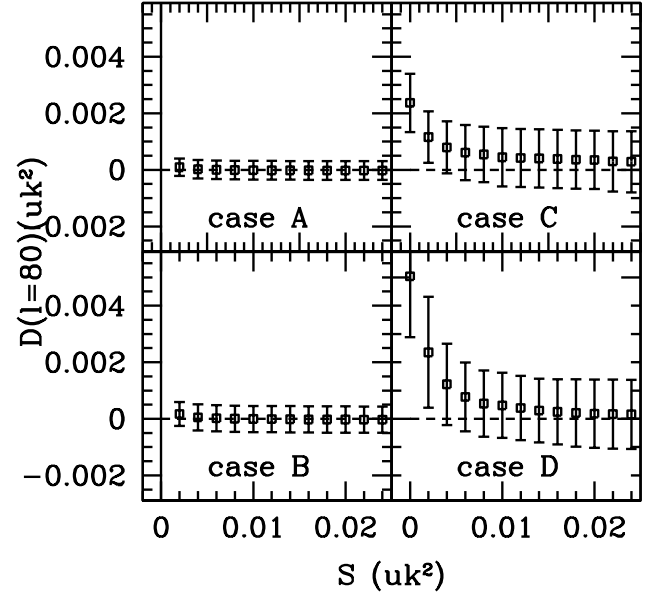


**Figure 5.** The null test result for the noise level  $\sigma_{\mathcal{D}}^{\text{inst}} = 10^{-3} \mu\text{K}^2$ . We set the signal as zero and check the ABS output. The  $\mathcal{S} = 0$  version of the ABS method fails the null test since by design it always returns positive value. But  $\mathcal{S}$  which passes the convergence test (Fig. 4) automatically passes the null test.

questions for future investigation. The statistical error, for each noise level, foreground and signal, is estimated using 200 realizations of instrument noises (but identical CMB and foregrounds). For all investigated foregrounds, signal and noise levels, our method faithfully extracts the input B-mode. It is unbiased even for high level of instrument noise  $\sigma_{\mathcal{D}}^{\text{inst}} \sim \mathcal{D}_{\text{B}}$ .

#### 4.1. Convergence test and self-calibration

The above results are obtained adopting  $\mathcal{S} = 20\sigma_{\mathcal{D}}^{\text{inst}}$ . We emphasize that such value of  $\mathcal{S}$  is not chosen arbitrarily. It is self-determined by the data, through the step 3 of the ABS method (§2.2). The choice of  $\mathcal{S}$  is not important when  $\sigma_{\mathcal{D}}^{\text{inst}} \ll \mathcal{D}_{\text{B}}$ . However, it will become important when  $\sigma_{\mathcal{D}}^{\text{inst}} \sim \mathcal{D}_{\text{B}}$ . For  $\mathcal{D}_{\text{B}} = 2 \times 10^{-3} \mu\text{K}^2$  and  $\sigma_{\mathcal{D}}^{\text{inst}} = 10^{-3} \mu\text{K}^2$ , Fig. 4 shows the ABS output adopting various shift parameter  $\mathcal{S}$ . For small value of  $\mathcal{S}$  systematic bias in  $\mathcal{D}_{\text{B}}$  can develop. At  $\mathcal{S} = 0$ , the systematic bias becomes greater than  $1\sigma$  for case C and D (Fig. 4). But with increasing  $\mathcal{S}$ , this bias vanishes eventually and the estimated  $\mathcal{D}_{\text{B}}$  converges. Hereafter we adopt  $\mathcal{S} = 20\sigma_{\mathcal{D}}^{\text{inst}}$ . Fig. 3 shows that this choice of  $\mathcal{S}$  returns unbiased result for all other cases of foregrounds and  $\mathcal{D}_{\text{B}}$ .

#### 4.2. Null test

We also carry out a null test of the ABS method by setting the input signal zero. The  $\mathcal{S} = 0$  version of ABS (Eq. 7) fails the null test since it always returns positive value. Furthermore, the output result can be very unstable (e.g. leftmost data points of Fig. 5). Fortunately with  $\mathcal{S} \sim 10\sigma_{\mathcal{D}}^{\text{inst}}$  that can pass the convergence test, the null test is also passed. This again demonstrates that step 3 of the ABS method is necessary. We address here

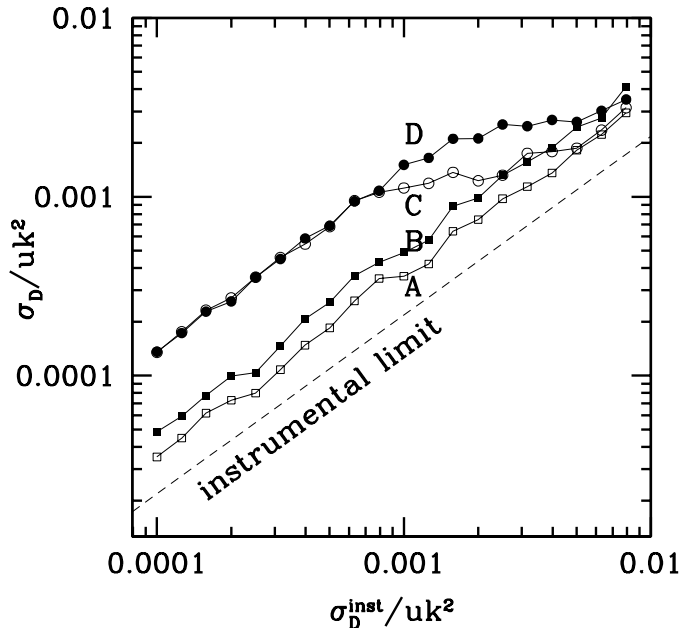


**Figure 6.** The dependence of the statistical error  $\sigma_{\mathcal{D}}$  on the instrument bandpower error  $\sigma_{\mathcal{D}}^{\text{inst}}$  per band.  $\sigma_{\mathcal{D}}$  at  $\ell \sim 80$  and survey configuration “F0” is shown for the foreground cases of A, B, C and D, respectively. The dash line is the instrumental limit  $\sigma_{\mathcal{D}}^{\text{inst}}/\sqrt{N_f(N_f+1)}/2$  which can only be achieved when foregrounds are negligible.

that the choice of  $\mathcal{S}$  does not induce extra uncertainty in the CMB measurement, because it is completely fixed by the data itself through the convergence test in §4.1.

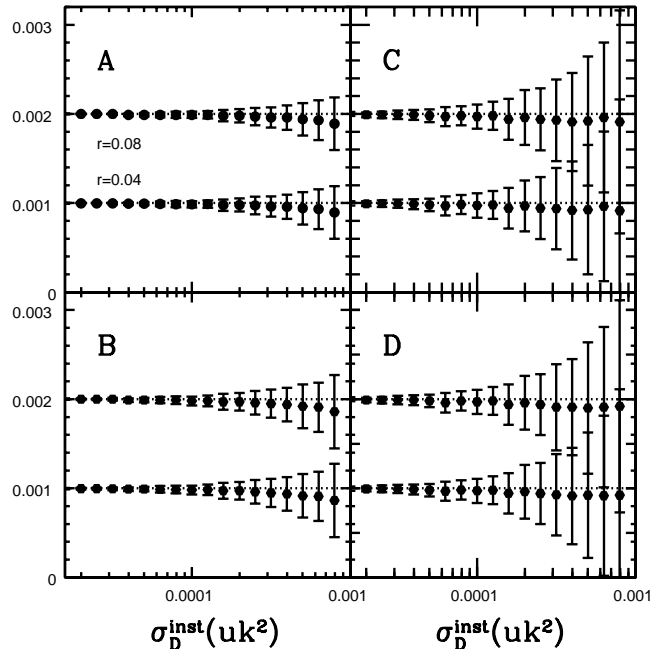
#### 4.3. Statistical errors

Fig. 6 plots the statistical error of the estimated  $\mathcal{D}_{\text{B}}$  as a function of instrument noise  $\sigma_{\mathcal{D}}^{\text{inst}}$ . Roughly speaking, the statistical error  $\sigma_{\text{B}} \propto \sigma_{\mathcal{D}}^{\text{inst}}$ . This is what we expect from our analytical prediction. Fig. 6 also compares  $\sigma_{\text{B}}$  with  $\sigma_{\text{min}} \equiv \sigma_{\mathcal{D}}^{\text{inst}}/\sqrt{N_f(N_f+1)}/2$ . The later is a lower bound of statistical error. It corresponds to the limit of no foreground contaminations in which we can simply average over all cross correlation measurements. The presence of foreground enlarges the statistical error, by a factor of  $\sim 2$  for case A/B and a factor of  $\sim 6$  for case C/D.

#### 4.4. Insensitivity to foregrounds

The above results also show that the recovery of B-mode by ABS is insensitive to the overall amplitude and spectral shape of galactic foregrounds. For example, case B has a factor of  $\sim 10$  larger dust contamination at  $\sim 150$  GHz band than case A. It also has a much flatter spectrum. Both would severely degrade the CMB extraction. However, the performance is almost as good as case A, without statistically significant bias. The only major difference is that the statistical error is about 40% larger (Fig. 6).

Furthermore, our ABS method also works when decorrelation of foregrounds at different frequencies exists (case C & D, Fig. 3). Case C & D have one more dust component, so one can not simply scale from high frequency maps to low frequency maps to remove dust



**Figure 7.** Similar to Fig. 3, but for  $\ell = 5$  around the reionization bump. The  $y$ -axis is the bandpower in unit of  $\mu\text{K}^2$ . Notice that, due to smaller B-mode at this scale and smaller instrumental noise (scales as  $\ell^{-1}$ ), we use different range of  $\sigma_{\mathcal{D}}$  to that in Fig. 3.

foreground. Our method nevertheless recovers the input B-mode, robustly and blindly. This demonstrates the advantage that the ABS method needs no assumptions on the number of independent foreground components.

Fig. 7 shows the test results at  $\ell \sim 5$  around the reionization bump (Fig. 7). Again the ABS successfully recovers the input B-mode. The signal, foregrounds and instrument noises at  $\ell \sim 5$  are very different to that at  $\ell \sim 80$ . The synchrotron and dust foregrounds are a factor of 5 and 3 larger, respectively. The B-mode signal is dominated by primordial gravitational wave B-mode, with an amplitude  $\lesssim 2 \times 10^{-3} \mu\text{K}^2$ . Therefore the overall B-mode signal to foreground ratio is a factor of  $\sim 10$  smaller than that at  $\ell \sim 80$ . Success of ABS for the  $\ell \sim 5$  then further demonstrates its insensitivity to foreground properties.

## 5. SURVEY REQUIREMENTS FOR UNBIASED MEASUREMENT

The success of ABS against the variety of foreground models, CMB signal and instrument noise levels investigated above is encouraging. Nonetheless, certain survey requirements have to be satisfied to achieve unbiased CMB measurement. If a survey is lack of necessary frequency coverage or is lack of necessary sensitivity, it may fail to correctly identify one or more foreground components. If such foregrounds are not orthogonal to CMB in frequency space, they will then lead to biased CMB estimation. The ABS method provides a specific diagnostic.

### 5.1. Bias induced by survey limitations

We demonstrate this point with the F1-4 frequency configuration. It turns out that ABS still remains unbiased for model A and B, for all relevant noise levels. Therefore for brevity we only show the tests results for foreground case C (Fig. 8).

The foreground case C for testing has a large synchrotron component, together with two dust components. The **F1** frequency configuration only covers frequency  $\gtrsim 90\text{GHz}$  and therefore has the poorest capability of separating the synchrotron component from others. Therefore should have the worst performance. The ABS output is unbiased only for very low instrument noise ( $\sigma_{\mathcal{D}}^{\text{inst}} \lesssim 3 \times 10^{-5} \mu\text{K}^2$ ). Systematic bias quickly grows with increasing instrument noise. When  $\sigma_{\mathcal{D}}^{\text{inst}} = 0.01 \mathcal{D}_{\text{B}} = 5 \times 10^{-5} \mu\text{K}^2$ , the bias is already 20% and the significance is  $1\sigma$  (foreground model C). The bias quickly increases to 40% when  $\sigma_{\mathcal{D}}^{\text{inst}} = 10^{-3} \mu\text{K}^2$ , and becomes statistically significant ( $2.5\sigma$ ). The fractional bias remains roughly a constant for larger  $\sigma_{\mathcal{D}}^{\text{inst}}$ , but its significance becomes weaker due to increasing statistical error.

This bias decreases with decreasing synchrotron amplitude, but it can still be statistically significant even when the synchrotron is only 10% of the observational upper limit. It is therefore dangerous to neglect the possible synchrotron foreground. Adding more frequency channels can significantly improve the situation (Fig. 8). Adding a 35 GHz band (the **F2** configuration), the bias vanishes when  $\sigma_{\mathcal{D}}^{\text{inst}} \lesssim 3 \times 10^{-4} \mu\text{K}^2$ . Further adding a 353 band (the **F3** configuration), the bias completely disappears and the performance of ABS is similar to the **F0** frequency configuration.

### 5.2. Survey requirements

The above tests show the following behaviors about the observed. (1) Incomplete frequency coverage alone may not necessarily lead to biased B-mode measurement, unless the instrument noise exceeds certain threshold  $\sigma_{\mathcal{D}}^{\text{thres}}$ . (2) The bias is positive, increases with  $\sigma_{\mathcal{D}}^{\text{inst}}$  until reaching a plateau. These behaviors, along with the values of  $\sigma_{\mathcal{D}}^{\text{thres}}$  and the bias, can be well understood within the framework of the ABS method. They actually reflect the limitation of a given CMB experiment.

We define

$$c_{\alpha} \equiv \frac{G_{\alpha}^2/\lambda_{\alpha}}{\sum_{\mu=1}^{M+1} G_{\mu}^2/\lambda_{\mu}}. \quad (13)$$

This is essentially the contribution of the  $\alpha$ -th eigenmode to the measurement of  $\mathcal{D}_{\text{B}} + \mathcal{S}$  (Eq. 2 & 3). If we miss this eigenmode, the ABS determined  $\mathcal{D}_{\text{B}}$  will be biased up by

$$\frac{\delta \mathcal{D}_{\text{B}}}{\mathcal{D}_{\text{B}}} = \frac{c_{\alpha}}{1 - c_{\alpha}} \times \left(1 + \frac{\mathcal{S}}{\mathcal{D}_{\text{B}}}\right) \equiv b_{\alpha} > 0. \quad (14)$$

The necessary condition of unbiased  $\mathcal{D}_{\text{B}}$  measurement by a given survey is that all eigenmodes of significant  $b_{\alpha}$  must be robustly identified. The S/N of the  $\alpha$ -th eigenmode is  $\tilde{\lambda}_{\alpha}$ . It is also the detection significance of this eigenmode. For our simplified case with identical instrument noise level across frequency bands,  $\tilde{\lambda}_{\alpha} = \lambda_{\alpha}/\sigma_{\mathcal{D}}^{\text{inst}}$ . Therefore, if  $\lambda_{\alpha} \lesssim \sigma_{\mathcal{D}}^{\text{inst}}$ , this eigenmode is overwhelmed by instrument noise and in-detectable. Inappropriate frequency coverage leads to the existence of such eigenmode with significant  $b_{\alpha}$  but tiny  $\lambda_{\alpha}$ . It then causes significant overestimation of  $\mathcal{D}_{\text{B}}$ .

Fig. 9 shows  $\lambda_{\alpha}$ - $c_{\alpha}$  in the **F0-F4** configurations for foreground case C. The CMB signal is  $\mathcal{D}_{\text{B}} = 5 \times 10^{-3} \mu\text{K}^2$ .

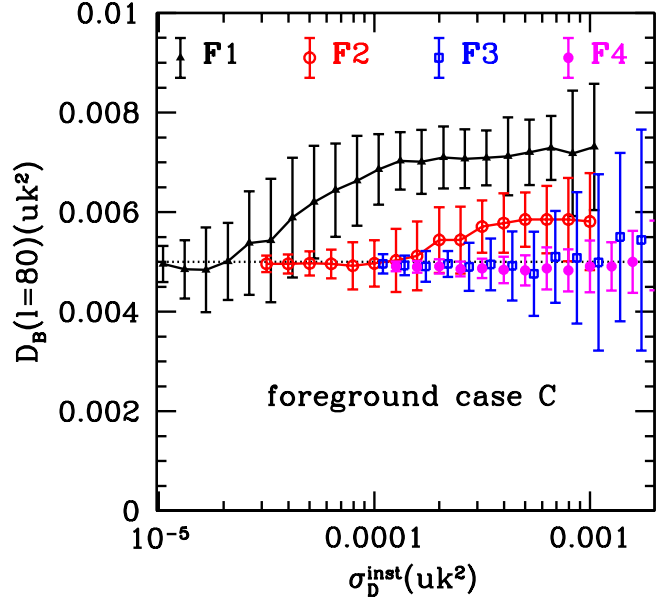


**Figure 8.** The impact of frequency coverage on CMB signal extraction. Incomplete frequency coverage (e.g. **F1**) and insufficient sensitivity cause failure in identifying certain eigenmodes significant for B-mode measurement (Fig. 9). This survey limitation causes bias in  $\mathcal{D}_{\text{B}}$ .

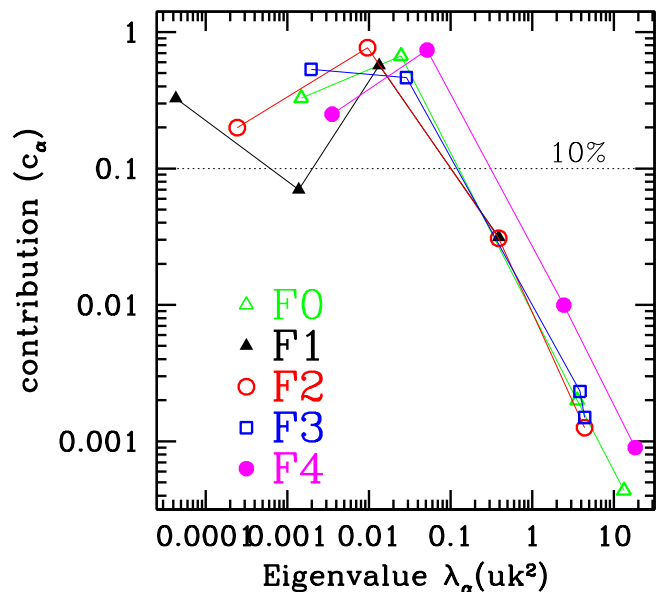


**Figure 9.** A diagnostic of unbiased B-mode extraction. The detection significance of the  $\alpha$ -th eigenmode is  $\lambda_{\alpha}/\sigma_{\mathcal{D}}^{\text{inst}}$ . If  $\lambda_{\alpha} \lesssim \sigma_{\mathcal{D}}^{\text{inst}}$ , this eigenmode becomes in-detectable. This results in a fractional systematic error of  $c_{\alpha}/(1 - c_{\alpha})$  in  $\mathcal{D}_{\text{B}}$ . Incomplete frequency coverage leads to the existence of physical eigenmodes with small  $\lambda_{\alpha}$ , but significant  $c_{\alpha}$ .

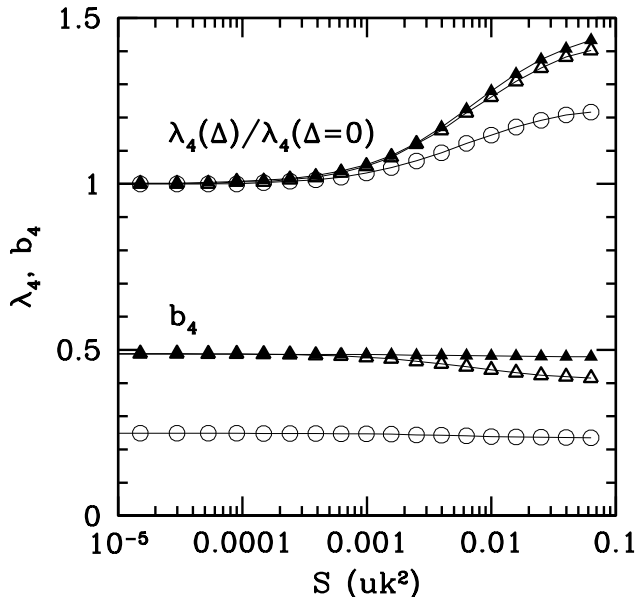


**Figure 10.** The dependence of the smallest eigenmodes on the shift parameter  $\mathcal{S}$ , for foreground model C and frequency configuration **F0-3**.

The shift parameter  $\mathcal{S} = 0$  so  $c_\alpha = b_\alpha$ . Fig. 10 shows the dependence of  $\lambda_\alpha$  and  $c_\alpha$  on the shift parameter  $\mathcal{S}$ .  $\mathcal{D}_{ij}$  of case C has  $M + 1 = 4$  physical eigenmodes. The first two are usually dominated by foregrounds and therefore have large eigenvalues. But due to the  $1/\lambda_\mu$  weighting in Eq. 2, their impacts on the B-mode extraction are automatically suppressed to a level negligible ( $b_\alpha \ll 1$ ). Usually both the third and fourth eigenmodes have significant  $c_\alpha$ , and therefore are important for B-mode extraction. The problem of **F1** is that the fourth eigenmode has a large  $c_4 = 0.33$  but a tiny  $\lambda_4 = 4.3 \times 10^{-5} \mu\text{K}^2$ . The operation of Eq. 7 with  $\mathcal{S} > 0$  changes this eigenvalue, but  $b_4$  is essentially unchanged (Fig. 10). Missing this eigenmode then biases  $\mathcal{D}_B$  up by  $b_4 \simeq 50\%$ . This explains the observed bias for the **F1** frequency configuration, when  $\sigma_{\mathcal{D}}^{\text{inst}} \gtrsim \lambda_4$  (Fig. 8).

Nevertheless,  $\mathcal{S} > 0$  benefits the determination of CMB B-mode. The eigenvalue increases with increasing  $\mathcal{S}$  (Fig. 10). Therefore this eigenmode becomes more significant against instrument noise. For fixed instrument noise, it leads to reduced systematic error.

Adding the 35 GHz band (**F2**) improves the identification of synchrotron foreground, reflecting as significantly larger  $\lambda_4 = 2.4 \times 10^{-4} \mu\text{K}^2$  and significantly smaller  $c_4 = 0.2$ . This significantly improves the situation, until  $\sigma_{\mathcal{D}}^{\text{inst}} \gtrsim \lambda_4$ , where a bias of  $b_4 \simeq 25\%$  develops. An extra 353 GHz band pushes all  $\lambda_\alpha > 10^{-3} \mu\text{K}^2$  and the systematic error essentially vanishes.

Adding more frequency bands further reduces the risk of more complicated foregrounds. Future experiments such as CORE, PRISM and PIXIE will have dozens or more frequency bands, and low instrument noise ( $\sigma_{\mathcal{D}}^{\text{inst}} \lesssim 10^{-4} \mu\text{K}^2$ ). Such high degree of redundancy would make

them safe for even more complicated foregrounds. We expect them to achieve unbiased and precise measurement of  $\mathcal{D}_B$  (e.g. **F4**, Fig. 8).

Therefore Eq. 13 & 14 can be useful for survey design. Given the fiducial foreground and survey configurations, these equations tell us whether this survey is sufficient for B-mode detection, what survey depth is required, and what the gain of adding extra frequency channels is.

## 6. CONCLUSION AND DISCUSSION

The simulated data used for our tests includes both synchrotron and thermal dust foreground and takes decorrelation of dust foreground into account. However, it does not include other possible foregrounds such as spinning dust, due to large uncertainty in their understandings. In future works we plan to include more foregrounds, consider more realistic (and therefore more complicated) instrumental noise, and redo the tests carried out in this paper. Nevertheless, since our method makes no assumption on foreground, the success of existing tests implies that it should also work with the existence of foregrounds other than synchrotron and thermal dust foregrounds.

Our ABS method applies when survey windows/masks exist, as discussed in the appendix. We then conclude that our method is applicable to general case of foregrounds for blind, yet accurate, extraction of CMB B-mode. It is also numerically stable against various instrument noise. It further provides a quantitative requirement (Eq. 13) for unbiased B-mode measurement, useful for design of future CMB experiments.

Our ABS method is significantly different to SMICA, other than sharing an identical goal to solve Eq. 1 for  $\mathcal{D}_B$ . (1) To our best knowledge, this is the first time that the analytical solution (Eq. 2) is discovered and the analytical B-mode extraction method based on it is constructed. It does not require multi-parameter fitting, which can be time consuming and numerically challenging. (2) our method works on individual  $\ell$  bin. It does not require assumptions on the scale dependence of foreground components (e.g. whether the foreground spectral dependence varies with  $\ell$ ).

Our method also works for blind measurements of CMB spectra distortion, E-mode polarization and the thermal SZ effect. Furthermore, it has important applications even in totally different areas. For example, it may serve as the ultimate solution to the original proposal of extracting cosmic magnification by counting galaxies (Zhang & Pen 2005). Yang & Zhang (2011); Yang et al. (2015) implemented this idea under the assumption of deterministic galaxy bias. With the ABS method, Yang et al. (2017) demonstrated that the stochastic galaxy bias can also be dealt with and the lensing power spectrum can be reconstructed without assumptions of galaxy bias. Given its excellent performance, other potential applications should be explored too.

## 7. ACKNOWLEDGMENTS

We thank Xuelei Chen, Xinjuan Yang and Yu Yu for useful discussions. This work was supported by the National Science Foundation of China (11653003, 11433001, 11621303, 11320101002) and National Basic Research Program of China (2015CB857001, 2013CB834900).

## APPENDIX

## APPENDIX A: THE DERIVATION OF THE ABS METHOD

## Uniqueness of solution

We first define vectors in frequency space of  $N_f$  dimensions,  $\mathbf{f}^{(\alpha)} \equiv (f_1^{(\alpha)}, \dots, f_{N_f}^{(\alpha)})$ . Without loss of generality, we absorb  $\mathcal{D}_\alpha$  into corresponding  $\mathbf{f}^{(\alpha)}$ . Suppose that  $(\sigma, \mathbf{h}^{(1)}, \dots, \mathbf{h}^{(M)})$  is also a set of solution to Eq. 1 & 8,

$$\mathcal{D}_{ij} = f_i^B f_j^B \sigma + \sum_{\beta=1}^M h_i^{(\beta)} h_j^{(\beta)}. \quad (\text{A1})$$

Then,  $\mathbf{h}^{(\beta)}$  must be linear combinations of the eigenvector  $\mathbf{E}$ s. Since  $\mathbf{E}$ s are linear combinations of vector  $\mathbf{f}^{(\alpha)}$  and  $\mathbf{f}^B$ ,  $\mathbf{h}^{(\beta)}$  must be linear combinations of  $\mathbf{f}^{(\alpha)}$  and  $\mathbf{f}^B$ ,

$$\mathbf{h}^{(\beta)} = \left[ \sum_{\alpha=1}^M R_{\alpha\beta} \mathbf{f}^{(\alpha)} \right] + B_\beta \mathbf{f}^B. \quad (\text{A2})$$

Here,  $R_{\alpha\beta}$  and  $B_\beta$  are constants to be determined. Plug the above relation into Eq. A1 and compare with Eq. 1 & 8, we obtain

$$\sum_{\beta} R_{\alpha\beta} R_{\gamma\beta} = \delta_{\alpha\gamma}, \quad \sum_{\beta} R_{\alpha\beta} B_\beta = 0, \quad \mathcal{D}_B - \sum_{\beta} B_\beta^2 = \sigma. \quad (\text{A3})$$

The first relation state that the matrix  $\mathbf{R}$  is orthogonal,  $\mathbf{R}^T \mathbf{R} = I$  where  $I$  is the unity matrix. Hence  $\det \mathbf{R} = \pm 1$ . Therefore

$$\det \mathbf{R} \neq 0 \ \& \ \mathbf{R} \cdot \mathbf{B} = 0 \Rightarrow \mathbf{B} = 0 \Rightarrow \sigma = \mathcal{D}_B. \quad (\text{A4})$$

We then prove that the solution to  $\mathcal{D}_B$  is unique.

In contrast, solutions to  $\mathbf{f}^{(\alpha)}$  are not unique, subject to transformation defined by  $\mathbf{R}$  with  $\det \mathbf{R} = \pm 1$ . Actually when  $\det \mathbf{R} = 1$ ,  $\mathbf{R}$  is the unitary rotation matrix operating in the  $M$  dimension frequency space. It is only after we fix the physics of each  $\mathbf{f}$ s, may we uniquely solve them.

Analytical Solution of  $\mathcal{D}_B$ 

From Eq. 1, we obtain  $E_{\mu\nu} = G_\mu G_\nu \mathcal{D}_B + F_{\mu\nu}$ . Here,  $F_{\mu\nu} \equiv \sum_{ij} E_i^{(\mu)} \mathcal{D}_{ij}^{\text{fore}} E_j^{(\nu)}$  and  $G_\mu \equiv \sum_i f_i^B E_i^{(\mu)}$ .  $E_{\mu\nu}$  is diagonal ( $E_{\mu\nu} = \lambda_\mu \delta_{\mu\nu}$ ), with order  $M+1$  and rank  $M+1$ . Moving  $G_\mu G_\nu \mathcal{D}_B$  to the l.h.s., we obtain

$$E_{\mu\nu} - G_\mu G_\nu \mathcal{D}_B = F_{\mu\nu}. \quad (\text{A5})$$

The rank of  $\mathbf{F}$  is  $M$ , smaller than its order  $M+1$ . As a result,

$$\det (E_{\mu\nu} - G_\mu G_\nu \mathcal{D}_B) = 0. \quad (\text{A6})$$

The Sylvester's determinant theorem states that for matrices  $\mathbf{A}$  ( $m \times n$ ),  $\mathbf{B}$  ( $n \times m$ ),  $\mathbf{X}$  ( $m \times m$ ) and unitary matrix  $\mathbf{I}_n$  ( $n \times n$ ),

$$\det(\mathbf{X} + \mathbf{A}\mathbf{B}) = \det(\mathbf{X}) \det(\mathbf{I}_n + \mathbf{B}\mathbf{X}^{-1}\mathbf{A}). \quad (\text{A7})$$

Eq. A6 then becomes

$$0 = \det(\mathbf{E} - \mathbf{G}\mathbf{G}^T \mathcal{D}_B) = \det(\mathbf{E}) (1 - \mathcal{D}_B \mathbf{G}^T \mathbf{E}^{-1} \mathbf{G}).$$

Since  $\det(\mathbf{E}) \neq 0$ , we prove Eq. 2. It also proves the uniqueness of the solution for  $\mathcal{D}_B$  from Eq. 1.

## The error estimation

The measured band powers are subject to instrumental noise. After subtracting the ensemble average from the diagonal elements, there will still be random noise  $\delta \mathcal{D}_{ij}^{\text{inst}}$  (with  $\langle \delta \mathcal{D}_{ij}^{\text{inst}} \rangle = 0$ ) on top of  $\mathcal{D}_{ij}$  of Eq. 1. In the limit of small perturbations,

$$\delta \lambda_\mu = \delta \mathcal{D}_{\mu\mu}, \quad \delta \mathbf{E}^{(\mu)} = \sum_{\nu \neq \mu} \frac{\delta \mathcal{D}_{\mu\nu}}{\lambda_\mu - \lambda_\nu} \mathbf{E}^{(\nu)}. \quad (\text{A8})$$

Here  $\delta \mathcal{D}_{\mu\nu} \equiv \sum_{ij} E_i^{(\mu)} \delta \mathcal{D}_{ij}^{\text{inst}} E_j^{(\nu)}$ . Correspondingly,

$$\delta G_\mu = \sum_{\nu \neq \mu} \frac{\delta \mathcal{D}_{\mu\nu}}{\lambda_\mu - \lambda_\nu} G_\nu, \quad \delta E_{\mu\nu} = \delta \lambda_\mu \delta_{\mu\nu}.$$

Here we have required the eigenvectors to be normalized to unity, and for that,  $E_{\mu\nu} = \lambda_\mu \delta_{\mu\nu}$ . We obtain by perturbing Eq. 2,

$$\frac{\delta\mathcal{D}_B}{\mathcal{D}_B^2} = - \sum_{\mu} (2\delta G_{\mu} \lambda_{\mu}^{-1} G_{\mu} - \lambda_{\mu}^{-2} \delta \lambda_{\mu} G_{\mu}^2) = - \sum_{\mu} \sum_{\nu \neq \mu} \frac{2\delta \mathcal{D}_{\mu\nu} G_{\mu} G_{\nu}}{(\lambda_{\mu} - \lambda_{\nu}) \lambda_{\mu}} + \sum_{\mu} \lambda_{\mu}^{-2} \delta \mathcal{D}_{\mu\mu} G_{\mu}^2. \quad (\text{A9})$$

We now symmetrize the first term on the right side of the above equation. We can switch between  $\mu \leftrightarrow \nu$  and take the average,

$$\frac{1}{2} \left( - \sum_{\mu} \sum_{\nu \neq \mu} \frac{2\delta \mathcal{D}_{\mu\nu} G_{\mu} G_{\nu}}{(\lambda_{\mu} - \lambda_{\nu}) \lambda_{\mu}} - \sum_{\nu} \sum_{\mu \neq \nu} \frac{2\delta \mathcal{D}_{\mu\nu} G_{\mu} G_{\nu}}{(\lambda_{\nu} - \lambda_{\mu}) \lambda_{\nu}} \right) = \sum_{\mu, \nu \neq \mu} \frac{\delta \mathcal{D}_{\mu\nu} G_{\mu} G_{\nu}}{\lambda_{\mu} \lambda_{\nu}}. \quad (\text{A10})$$

Therefore

$$\frac{\delta\mathcal{D}_B}{\mathcal{D}_B^2} = \sum_{\mu, \nu} \frac{\delta \mathcal{D}_{\mu\nu} G_{\mu} G_{\nu}}{\lambda_{\mu} \lambda_{\nu}}. \quad (\text{A11})$$

Notice that now the sum includes  $\mu = \nu$  pairs.  $\sigma_{\mathcal{D}}^2 \equiv \langle \delta \mathcal{D}_B^2 \rangle$  can be derived using the following relation,

$$\langle \delta \mathcal{D}_{\mu\nu} \delta \mathcal{D}_{\rho\sigma} \rangle = \sum_{ijklm} E_i^{(\mu)} E_j^{(\nu)} E_k^{(\rho)} E_l^{(\sigma)} \langle \delta \mathcal{D}_{ij} \delta \mathcal{D}_{km} \rangle = \frac{1}{2} \sum_{ij} E_i^{(\mu)} E_j^{(\nu)} \sigma_{\mathcal{D},i}^{\text{inst}} \sigma_{\mathcal{D},j}^{\text{inst}} (E_i^{(\rho)} E_j^{(\sigma)} + E_i^{(\sigma)} E_j^{(\rho)}).$$

The last expression uses the relation  $\langle \delta \mathcal{D}_{ij} \delta \mathcal{D}_{km} \rangle = \sigma_{\mathcal{D},i}^{\text{inst}} \sigma_{\mathcal{D},j}^{\text{inst}} (\delta_{ik} \delta_{jm} + \delta_{im} \delta_{jk})/2$ . The prefactor 1/2 ensures that  $\langle (\delta \mathcal{D}_{ii})^2 \rangle = (\sigma_{\mathcal{D},i}^{\text{inst}})^2$ . For the simplified case  $\sigma_{\mathcal{D},1}^{\text{inst}} = \sigma_{\mathcal{D},2}^{\text{inst}} = \dots = \sigma_{\mathcal{D}}^{\text{inst}}$ , we have

$$\sigma_{\mathcal{D}} = \sigma_{\mathcal{D}}^{\text{inst}} \left( \sum_{\mu} \frac{G_{\mu}^2}{\lambda_{\mu}^2} \mathcal{D}_B^2 \right). \quad (\text{A12})$$

For general case of  $\sigma_{\mathcal{D}}^{\text{inst}}$  varying with frequency, it is

$$\sigma_{\mathcal{D}} = \sum_{\mu} \frac{\tilde{G}_{\mu}^2}{\tilde{\lambda}_{\mu}^2} \mathcal{D}_B^2. \quad (\text{A13})$$

The above two results are for the case of  $\mathcal{S} = 0$ . When  $\mathcal{S} \neq 0$ , the factor  $\mathcal{D}_B$  shall be replaced by  $\mathcal{D}_B + \mathcal{S}$ .

## APPENDIX B: THE APPLICABILITY OF ABS IN REAL SURVEYS

The ABS method has been derived under simplified situations. So an immediate question is whether it can be applied to real CMB surveys. The main text incorporate the fact that different frequency bands have different instrument noises and therefore should have different weights to obtain optimal measurement of CMB B-mode. There are other complexities. The measured CMB is smoothed over the beam, which depends on frequency. The masks in general vary with frequency. Even if we adopt identical mask for all frequency bands, the interplay between beam and mask causes decorrelation of the CMB signal in different frequency bands. Here we outline a procedure to apply the ABS method with the presence of these complexities.

- **Step 1.** We smooth all maps to a fiducial beam  $B^f(\theta)$ , before masking. This beam should be identical for all frequency bands. It should be homogeneous and isotropic, for the convenience of later process. Therefore it should only depend on the angle  $\theta$  between the pixel position ( $\hat{n}_{\text{pixel}}$ ), and the sky position ( $\hat{n}$ ) where the signal comes from. If the actual beams are also homogeneous, this step can be done efficiently in harmonic space by multiplying  $a_{lm}$  of the  $i$ -th frequency band by  $B^f(l)/B_i(l, m)$ . Here  $B_i(l, m)$  is the beam of the  $i$ -th frequency band, which can be anisotropic. In reality, the beam is in general inhomogeneous (depending on  $\hat{n}_{\text{pixel}}$ ) and this step shall be done pixel by pixel.
- **Step 2.** We chose and apply a common mask  $M(\hat{n}_{\text{pixel}})$  for all frequency maps.
- **Step 3.** We then measure the cross band power between these smoothed/masked maps  $\mathcal{D}_{ij}^{\text{S+M}}(\ell)$ . We subtract the ensemble average of the instrument noise power spectra from the diagonal elements. We also estimate the r.m.s. of the residual instrument noise  $\sigma_{\mathcal{D},i}^{\text{inst}}(\ell)$  in each map.
- **Step 4.** We then weigh  $\mathcal{D}_{ij}^{\text{S+M}}$  by  $\sqrt{\sigma_{\mathcal{D},i}^{\text{inst}} \sigma_{\mathcal{D},j}^{\text{inst}}}$  and obtain essentially the S/N matrix  $\tilde{\mathcal{D}}_{ij}$ . The ABS method then directly applies to

$$\tilde{\mathcal{D}}_{ij} \equiv \frac{\mathcal{D}_{ij}^{\text{S+M}}}{\sqrt{\sigma_{\mathcal{D},i}^{\text{inst}} \sigma_{\mathcal{D},j}^{\text{inst}}}} = \tilde{f}_i^B \tilde{f}_j^B \mathcal{D}_B^{\text{S+M}} + \tilde{\mathcal{D}}_{ij}^{\text{fore}}. \quad (\text{B1})$$

Here,  $\tilde{f}_i^B \equiv f_i^B / \sqrt{\sigma_{\mathcal{D},i}^{\text{inst}}}$ .  $\mathcal{D}_B^{\text{S+M}}$  is the CMB band power, with beam  $B^f(\theta)$  and mask  $M$ . The ABS method directly applies to the above equation and solves for  $\mathcal{D}_B^{\text{S+M}}$ .

- **Step 5.** It is then the standard procedure to deconvolve  $\mathcal{D}_B^{\text{S+M}}$  for  $\mathcal{D}_B$  (e.g. Hivon et al. (2002)).

In particular, step 1 (smoothing) and step 2 (masking) are not interchangeable. Otherwise the CMB signal in different maps will not be linearly proportional to each other and the signal term in Eq. B1 does not have the form  $\propto \tilde{f}_i^B \tilde{f}_j^B$ .

#### REFERENCES

- Abazajian, K. N., Adshead, P., Ahmed, Z., et al. 2016, ArXiv e-prints, arXiv:1610.02743
- André, P., Baccigalupi, C., Banday, A., et al. 2014, JCAP, 2, 006
- BICEP2 Collaboration, Ade, P. A. R., & et al. 2014, Physical Review Letters, 112, 241101
- BICEP2/Keck and Planck Collaborations, Ade, P. A. R., Aghanim, N., et al. 2015, Physical Review Letters, 114, 101301
- Bock, J., Cooray, A., Hanany, S., et al. 2008, ArXiv e-prints, arXiv:0805.4207
- Cardoso, J.-F., Le Jeune, M., Delabrouille, J., Betoule, M., & Patanchon, G. 2008, IEEE Journal of Selected Topics in Signal Processing, 2, 735
- Delabrouille, J., Cardoso, J.-F., & Patanchon, G. 2003, MNRAS, 346, 1089
- Delabrouille, J., de Bernardis, P., Bouchet, F. R., et al. 2017, ArXiv e-prints, arXiv:1706.04516
- Draine, B. T., & Hensley, B. 2012, ApJ, 757, 103
- Gandilo, N. N., Ade, P. A. R., Benford, D., et al. 2016, ArXiv e-prints, arXiv:1607.06172
- Grayson, J. A., Ade, P. A. R., Ahmed, Z., et al. 2016, ArXiv e-prints, arXiv:1607.04668
- Hivon, E., Górski, K. M., Netterfield, C. B., et al. 2002, ApJ, 567, 2
- Inoue, Y., et al. 2016, arXiv:1608.03025
- Kamionkowski, M., Kosowsky, A., & Stebbins, A. 1997, Physical Review Letters, 78, 2058
- Keisler, R., Hoover, S., Harrington, N., et al. 2015, ApJ, 807, 151
- Kogut, A., Fixsen, D. J., Chuss, D. T., et al. 2011, JCAP, 7, 025
- Li, H., Li, S.-Y., Liu, Y., et al. 2017, ArXiv e-prints, arXiv:1710.03047
- Matsumura, T., Akiba, Y., Borrill, J., et al. 2014, Journal of Low Temperature Physics, 176, 733
- Planck Collaboration, Ade, P. A. R., Aghanim, N., et al. 2011, A&A, 536, A20
- Planck Collaboration, Adam, R., Ade, P. A. R., et al. 2015a, ArXiv e-prints, arXiv:1502.05956
- . 2015b, ArXiv e-prints, arXiv:1502.01588
- Planck Collaboration, Ade, P. A. R., Aghanim, N., et al. 2015c, ArXiv e-prints, arXiv:1506.06660
- Planck Collaboration, Ade, P. A. R., Alves, M. I. R., et al. 2015d, A&A, 576, A107
- Planck Collaboration, Aghanim, N., Ashdown, M., et al. 2016a, ArXiv e-prints, arXiv:1606.07335
- Planck Collaboration, Adam, R., Ade, P. A. R., et al. 2016b, A&A, 586, A133
- Poh, J., & Dodelson, S. 2016, ArXiv e-prints, arXiv:1606.08922
- Remazeilles, M., Dickinson, C., Eriksen, H. K. K., & Wehus, I. K. 2016, MNRAS, 458, 2032
- Seljak, U. 1997, ApJ, 482, 6
- Seljak, U., & Zaldarriaga, M. 1997, Physical Review Letters, 78, 2054
- Starobinskiĭ, A. A. 1979, Soviet Journal of Experimental and Theoretical Physics Letters, 30, 682
- Tegmark, M., de Oliveira-Costa, A., & Hamilton, A. J. 2003, Phys. Rev. D, 68, 123523
- Thornton, R. J., Ade, P. A. R., Aiola, S., et al. 2016, ArXiv e-prints, arXiv:1605.06569
- Yang, X., Zhang, J., Yu, Y., & Zhang, P. 2017, ArXiv e-prints, arXiv:1703.01575
- Yang, X., & Zhang, P. 2011, MNRAS, 415, 3485
- Yang, X., Zhang, P., Zhang, J., & Yu, Y. 2015, MNRAS, 447, 345
- Zhang, P., & Pen, U.-L. 2005, Physical Review Letters, 95, 241302